Sensing and Imaging (2018) 19:21
https://doi.org/10.1007/s11220-018-0204-0

ORIGINAL PAPER

Design of a Low-Cost Thermal Dispersion Mass Air Flow (MAF) Sensor

Marcus A. Horning[1] · **Rikesh Shakya**[1] · **Nathan Ida**[2]

Received: 4 June 2017 / Revised: 30 April 2018
© Springer Science+Business Media, LLC, part of Springer Nature 2018

Abstract

There is a need for a low-cost sensor to be used in many practical applications, such as the control of the air–fuel ratio in combustion burners, which measures the mass flow rate of fluid. This paper focuses on the design, calibration, and testing of a mass flow sensor operating on the principle of thermal dispersion. The developed sensor implements a digital proportional-integral controller which regulates the body temperature of a heated element, recognized as a thermistor, located in the stream of the fluid flow to a constant difference with respect to the ambient air temperature. The power dissipated by this heated element was referenced to known mass flow rates of air to determine the relationship between the dissipated power and ambient temperature to the measured mass flow rate. The inclusion of air flow conditioners, which filtered unwanted debris and delivered a more laminar air flow, was imperative to the success of the design. The designed sensor was proven to measure the incoming mass air flow through a duct, in the presence of moderate disturbances in the intake air pipe and for a wide range of ambient air temperatures, with a maximum full-scale error of 5.5% and a range up to 80 kg/h.

This work was supported in part by the Wright Center for Sensor System Engineering (WCSSE) and by the R.W. Beckett Corporation.

✉ Marcus A. Horning
mao17@zips.uakron.edu

Rikesh Shakya
rs156@zips.uakron.edu

Nathan Ida
ida@uakron.edu

[1] The University of Akron, Akron, OH 44325, USA

[2] Electrical and Computer Engineering, The University of Akron, Akron, OH 44325, USA

Published online: 21 June 2018

Keywords Combustion efficiency · Fuel–air ratio · Laminar fluid flow · Mass air flow measurement · PI digital controller · Sensor · Thermal dispersion · Thermistor

1 Introduction

A gas flow meter is an instrument that measures the flow rate of gas through a duct. Flow meters are broadly divided into two categories: volumetric flow rate meters and mass flow rate meters. Volumetric flow rate meters measure the volume of the gas passing through the device per unit time. With knowledge of the temperature and pressure of the gas, the density of the gas can be computed such that the mass flow rate of the gas can be determined. On the contrary, mass flow rate meters measure the mass of the gas passing through the device per unit time [1, 2]. Unlike volumetric flow meters, mass flow meters intrinsically measure the mass flow rate of gas without knowledge of gas temperature, pressure, viscosity and altitude.

Different applications of gas flow measurement are employed in the automobile industry [3, 4, 5], heating industry [6], research experiments [7], process controls, and controlling air pollution. In the automobile industry, the control of the fuel–air ratio in the combustion process for the engine is of major importance. Maintaining the optimal ratio is vital for optimizing fuel economy and minimizing the harmful pollutants in the exhaust gas. Similar to its application in the automotive industry, the mass air flow meter is utilized in the heating industry to control the flue-gas oxygen ratio. By maintaining an ideal ratio, the combustion efficiency is optimized and the harmful components in the flue gas are reduced. In process controls, when measurement of the amount of different gases is critical, the mass flow meter is a crucial sensor.

This paper focuses on the design of a low-cost mass air flow sensor which operates on the principle of thermal dispersion. The developed sensor is intended for applications where a fast time response of sensor measurements is not critical, such as fuel–air ratio control in combustion burner systems. Unlike traditional mass air flow sensors operating on the principle of thermal dispersion which use a hot wire as the heating element, the innovative sensor documented in this paper utilizes thermistors. This exploits the thermistor's ability to not only provide heat by applying electrical power to its terminals, but also to have its resistance inherently change in relation to the thermistor's body temperature.

2 Theory of Operation

The operation of thermal dispersion air flow meters is based on the principle of convective heat transfer from a heated surface to the stream of fluid flowing across it. These meters directly measure mass flow rate, as opposed to the volumetric flow rate, as it is molecules that bear mass and carry away heat from the heated surface. The implementation of an electrically resistive element which possesses a high temperature coefficient of resistance is fundamental to the functioning of the sensor. When this element is heated and an electrical voltage is applied to its terminals, the

resulting electrical current through this heated component correlates to the mass of air flowing across it. As proven later in the present section, the electrical power dissipated by the heated sensor element is the most reliable electrical parameter that corresponds to the mass air flow rate.

There are two common types of thermal dispersion mass flow sensors: constant power type and constant temperature difference type [8]. Each of these require knowledge of the body temperature of the heated element and the ambient air temperature. Constant power type thermal flow meters are based on monitoring the temperature difference between the body temperature of the heated element and the ambient air temperature while supplying constant power to the heated element. The temperature difference is inversely proportional to mass flow rate of the fluid stream that passes the heated element. The second type of mass air flow meter maintains a constant temperature differential between the body temperature of the heated element and the ambient temperature [9]. The power dissipated by the heated element to maintain this temperature differential is proportional to the mass flow rate of the fluid stream that passes the heated element.

The first law of thermodynamics is applied to get a mathematical expression relating the electrical power dissipated by the heated element to the mass flow rate of fluid flowing across it. According to the first law of thermodynamics, the energy input in the form of electrical power to the heated element must be equal to the energy stored in the element and the heat lost due to conduction, convection, and radiation [10]. Mathematically, the heat balance equation for the heated element can be written as

$$P_e = \dot{Q}_{fconv} + \dot{Q}_{conv} + \dot{Q}_{cond} + \dot{Q}_{rad} + \dot{Q}_{stored} \tag{1}$$

where P_e is the electrical power input to the heated element, $\dot{Q}_{fconv}$ is forced convective heat transfer rate, $\dot{Q}_{conv}$ is natural convective heat transfer rate, $\dot{Q}_{cond}$ is conductive heat transfer from the heated element to the connecting sensor body,$\dot{Q}_{rad}$ is the radiation heat transfer rate, and $\dot{Q}_{stored}$ is the heat storage rate. The term $\dot{Q}_{cond}$ contributes to 10–15% of the total heat loss [10]. For simplicity, this term is neglected in the analysis. The natural convective heat transfer rate can be ignored as it is significant only at very low flow velocities. The radiation heat transfer rate is very small and it can also be ignored [11]. When the temperature differential is at steady state, the heat energy storage rate also becomes zero. Therefore, the simplified heat balance equation for the heated sensor can be approximated as

$$P_e = \dot{Q}_{fconv}. \tag{2}$$

The convective heat loss rate, calculated using Newton's law of cooling, can be expressed as

$$\dot{Q}_{fconv} = h_h \cdot A_h \cdot \left(T_h - T_a\right) \tag{3}$$

where A_h is the heat transfer surface area, T_h is the body temperature of the heated element, T_a is the ambient temperature, and h_h is the equivalent convective heat transfer coefficient. The equivalent convective heat transfer coefficient [12] is given by

$$h_h = h/\left(1 + h \cdot A_h \cdot R_s\right) \tag{4}$$

where R_s denotes the skin resistance and h represents the convective film heat transfer coefficient. Skin resistance is the thermal resistance of the intervening circuit board layers surrounding the heated element. The effect of skin resistance results in reduction in the sensitivity of the flow meter's output signal, and is more pronounced at higher mass flow rates. The skin resistance was assumed to be zero for further calculations as it is more pronounced at higher mass flow rates and the sensor under study is designed for small mass flow rates. Additionally, the heated element used in the mass flow meter is not surrounded by any additional layer of material or a sheath, but it is directly in contact with the air flow on all sides of the leg except the side it is laid on the circuit board.

The convective film heat transfer coefficient for the heated element is given by

$$h = k \cdot Nu/L \tag{5}$$

where k is the thermal conductivity of the fluid, Nu is the Nusselt number, and L is the characteristic length of the heated sensor. After substituting (4) and (5) into (3), the forced convective heat transfer rate can be rewritten as

$$\dot{Q}_{fconv} = k \cdot Nu \cdot A_h/L \cdot \left(T_h - T_a\right). \tag{6}$$

The Nusselt number can be written as a function of Reynolds number and the Prandtl number [10] given that the speed of air in the sensor's intake pipe is less than one-third the speed of sound, the air had negligible compressibility effects, and the flow is not in a vacuum. These values depend upon the flow velocity and the temperature-dependent fluid properties [11]. The general expression for Nu in variable gas temperature mass flow sensor [10] is given by

$$\mathrm{Nu} = \mathrm{A} + \mathrm{B} \cdot \mathrm{Pr}^{0.33} \cdot \mathrm{Re}^{n} \tag{7}$$

where, A, B and n are the constants that are determined during flow calibration. The Reynolds number is a dimensionless quantity that helps predict the fluid flow pattern, and is defined by the fluid density, fluid velocity, and the absolute viscosity of the air. These parameters are denoted by ρ,$\dot{m}$, and μ, respectively. The expression for the Reynolds number is given as

$$\mathrm{Re} = \rho \dot{m} L/\mu. \tag{8}$$

By rearranging the formula which is determined by substituting (2), (7), and (8) into (6), the mass flow of air in the meter [10] can be written as

$$\dot{m} = \mu \left[\frac{P_e(T_h - T_a) - \mathrm{A}k}{\mathrm{B}kPr^{0.33}}\right]^{1/n}. \tag{9}$$

At a specific ambient temperature and with the other parameters held constant, (9) shows that the mass flow rate is related to electrical power applied to the heated element. Additionally, a numerical relationship can be determined experimentally

from the calibration curve of mass flow rate versus electrical power applied to the heated element. Furthermore, since fluid conductivity and viscosity are temperature dependent, the mass flow rate of the fluid is dependent on the ambient temperature in addition to the difference between the body temperature of the heated sensor and the ambient air temperature [8, 13].

There are various sources of errors which effect the output of the sensor. A common source of error is caused by differences between the temperature of the gas inside the sensor conduit and the environment temperature outside of the sensor conduit. Due to the temperature differential, heat is conducted from the stem of the sensor to the outside and within the two stems of the sensor. This conduction phenomenon is known as stem conduction [12], and is dependent upon the mass flow rate. Figure 4b, c illustrate this effect by highlighting the sensor "stem" of the heated thermistor in relation to the gas and environment temperatures.

3 Applied Methodology

A thermal dispersion mass air flow sensor was designed in which a thermistor was employed as the hot element. The sensor utilized a microprocessor to implement a digital proportional-integral (PI) controller which maintained a 55 °C temperature differential between the heated thermistor body temperature and ambient temperature. This algorithm determined the desired power, and the associated voltage, which was applied to the heated thermistor. Additionally, the microprocessor was used to calculate the power dissipated on the thermistor with knowledge of the measured electrical current through and the voltage across the thermistor. The sensor was then calibrated by referencing the dissipated power and ambient temperature to known flow rates.

In order to increase the operational temperature range of the sensor and improve accuracy, the sensor employed two heated thermistors with different base resistances. Two common emitter amplifiers were used to enable the appropriate heated thermistor based on the ambient temperature. The schematic depicting the control and measurements circuit is shown in Fig. 1. The schematic of the gas temperature measurements circuit is shown in Fig. 2. The software flow chart depicting the high-level operation of the sensor is shown in Fig. 3.

The voltage and current applied to the heated thermistor are determined by

$$V_{Therm} = V_{Meas} - V_{CE} - R_8 \cdot I_{Therm} \tag{10}$$

$$I_{Therm} = \frac{R_{10}}{R_9 \cdot R_8} \cdot I_{Meas} \tag{11}$$

where V_{CE} is the collector-emitter voltage of transistors Q2 and Q3. The resistance of the heated thermistor, calculated from the voltage and current measurements, is related to the temperature of the thermistor body. The expressions, derived from the Steinhart-Hart equation and approximations of a NTC thermistor, which represent the temperature are given as

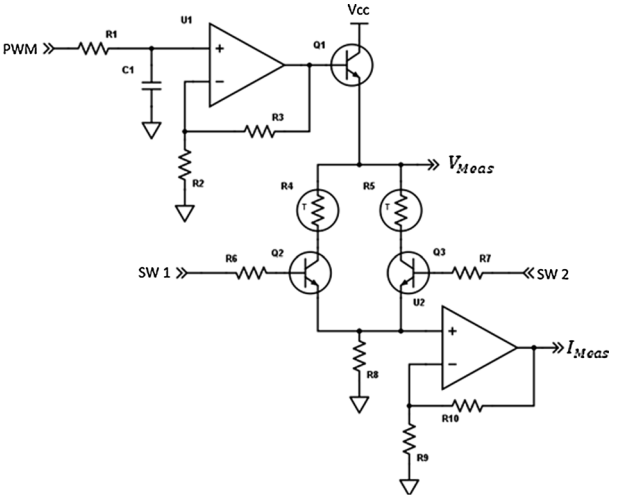

Fig. 1 Schematic-control and measurements circuit

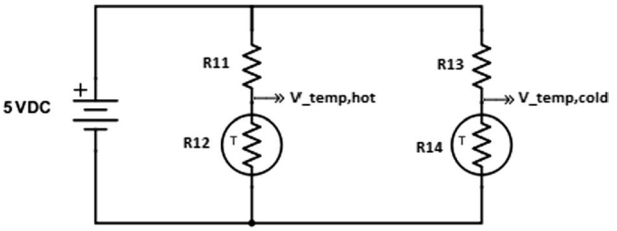

Fig. 2 Schematic-gas temperature measurements circuit

$$T = \frac{B}{\ln\left(R/r_{\infty}\right)} \tag{12}$$

$$r_{\infty} = R_0 \cdot e^{-B/T_0} \tag{13}$$

where T is the temperature, R is the resistance, B is the thermistor specific parameter, and R_0 is the resistance at temperature $T_0 = 298.15$ K. The thermistors utilized in the measurement of the gas temperature can be determined from the same expressions above. The voltage across the thermistors are directly measured, whereas the current can be easily calculated since the voltage supply and resistor are both fixed. Two thermistors with different base resistances were implemented to improve the accuracy across the entire temperature range.

Design of the digital controller requires knowledge of the model of the system. The system model representing the heating of a thermistor is given by

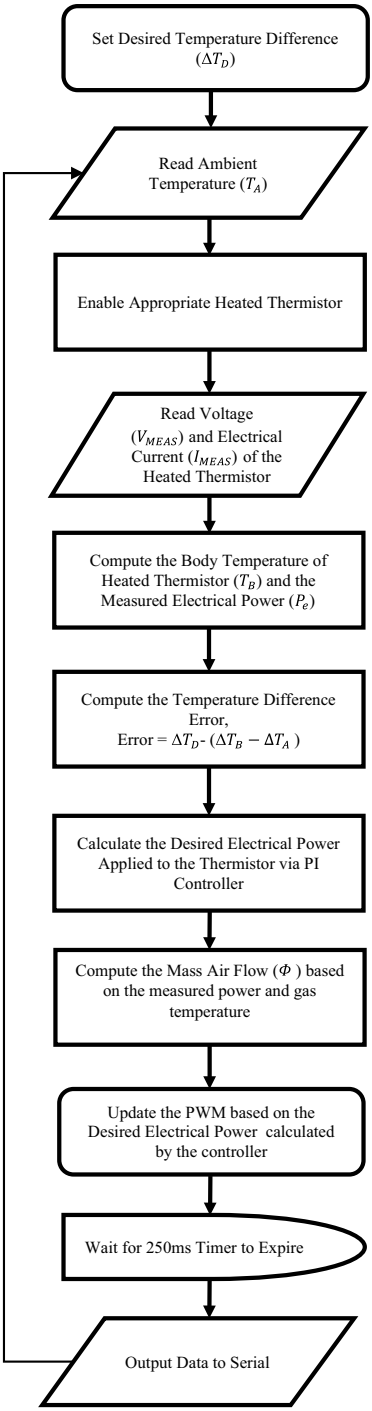

Fig. 3 High-level software flow chart

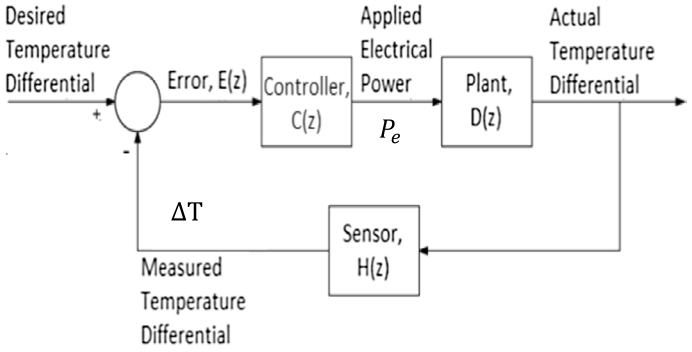

Fig. 4 Control system block diagram

$$P_e = V \cdot I = \delta_{th} \cdot \left(T - T_A\right) + C_{th} \cdot dT/dt \tag{14}$$

where P_e is the applied electrical power, δ_{th} is the lumped dissipation factor of the thermistor, T_A is the ambient temperature, T represents the body temperature of the thermistor, C_{th} depicts the heat capacity of the thermistor, and dT/dt is the change in the thermistor's body temperature with respect to time. Assuming that the ambient temperature is constant, the system transfer function relating the temperature differential to the applied power is

$$C(s) = \frac{\Delta T}{P_e} = 1/\left(C_{th} \cdot s + \delta_{th}\right) \tag{15}$$

where $\Delta T = T - T_A$ is the temperature differential. This system is considered stochastic because the value of the dissipation factor of the thermistor is dependent on the mass flow rate of air flowing across its surface. Therefore, the integral component of the controller is necessary to eliminate the steady-state error. A digital PI controller was chosen, where the proportional and integral gains were determined with an iterative method while observing the sensor properties. Using this method, the exact models of D(z) and H(z) did not need to be known. The control block diagram is illustrated in Fig. 4. The difference equation representing the controlling is given as

$$P_e = K_p \cdot e(k) + Ki \cdot e_i(k) + P_0 \tag{16}$$

where $K_p = 1/1200$ and $Ki = 1/1000$. This model was determined for a nominal system input,P_0, of 0.20 W for the operating conditions of a mass air flow rate of

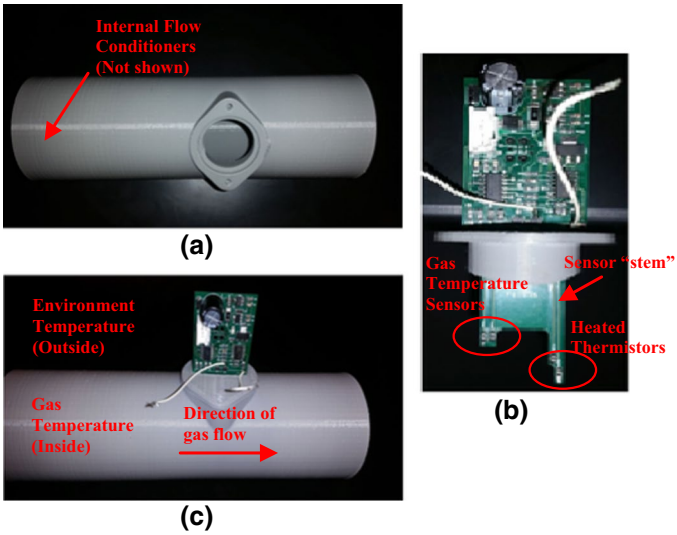

Fig. 5 **a** Main housing assembly, **b** sensor insert, **c** complete assembly

45 kg/h and a gas temperature of 65 °F. The error signal, $e(k)$, and integrated error, $e_i(k)$, are determined by

$$e(k) = \Delta T_{desired} - \Delta T \tag{17}$$

$$e_i(k) = e_i(k-1) + \frac{T_s}{2}[e(k) - e(k-1)] \tag{18}$$

where $\Delta T_{desired}$ is the desired temperature difference between the thermistor body temperature and the gas temperature, ΔT is the measured temperature difference, and $T_s = 250$ ms is the sampling time.

The PWM signal corresponding to the desired electrical power dissipated by the heated thermistor was calculated according to

$$PWM = \frac{(P_e/I_{Meas} + I_{Meas} \cdot R_8 + V_{CE} + V_{BE})}{K \cdot V_{cc}} \tag{19}$$

where V_{BE} is the base-emitter voltage of transistor Q1, V_{CE} is the collector-emitter voltage of Q2 and Q3, K is the gain of the non-inverting operational amplifier denoted U1, and V_{cc} is the supply voltage.

For accurate measurements, thermal dispersion flow sensors rely on the incoming flow to be laminar. Therefore, much consideration was done to ensure that the incoming flow was properly conditioned. The main housing assembly, which is illustrated in Fig. 5a, enclosed two honeycomb-style flow straighteners and a wire mesh. These functioned to not only straighten the air flow path, but also to remove any

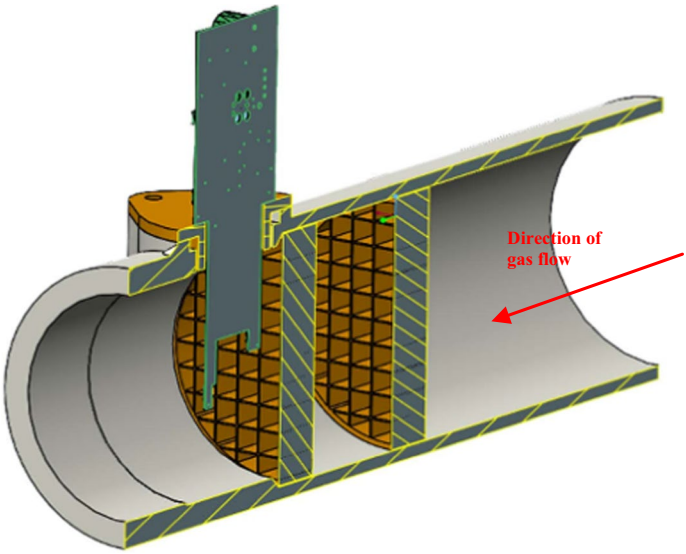

Fig. 6 CAD model

large debris from disrupting the air flow path. The sensor insert and the complete assembly are shown in Fig. 5b, c, respectively. Figure 6 illustrates a CAD model of a cross-section.

4 Results

The developed MAF sensor was calibrated with a known flow rate, which was determined with a reliable flow meter. The calibration involved computing the power dissipated by the heated thermistor, and determining its relationship with the actual mass flow rate. In addition to the mass flow rate of air, the power dissipated by the heated thermistor is also dependent on the ambient temperature of the surroundings. Using curve fitting techniques, the flow rate of air measured by the MAF sensor, denoted by $\boldsymbol{\Phi}$, is represented by

$$\boldsymbol{\Phi}\left(P_e, T_A\right) = a\left(T_A\right) \cdot P_e^2 + b\left(T_A\right) \cdot P_e + c\left(T_A\right) \tag{20}$$

where $a\left(T_A\right), b\left(T_A\right)$, and $c\left(T_A\right)$ are the ambient temperature dependent coefficients of the second order function. The ambient temperature and electrical power dissipated by the heated thermistor are represented by T_A and P_e, respectively.

The power dissipated by the heated thermistor was recorded for various flow rates of air. Figure 7 shows the power dissipated versus mass flow rate of air for ambient temperatures between 46 and 140 °F, whereas Fig. 8 shows the power dissipated versus mass flow rate of air for ambient temperatures between −40 and 46 °F.

The collected data was analyzed to determine the coefficients $a\left(T_A\right), b\left(T_A\right)$, and $c\left(T_A\right)$ and the equations representing the flow of air were found to be

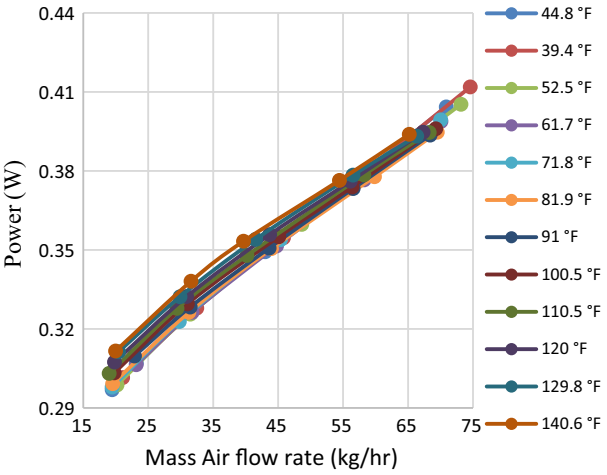

Fig. 7 Measured electrical power versus mass flow rate for ambient temperatures of 46–140 °F

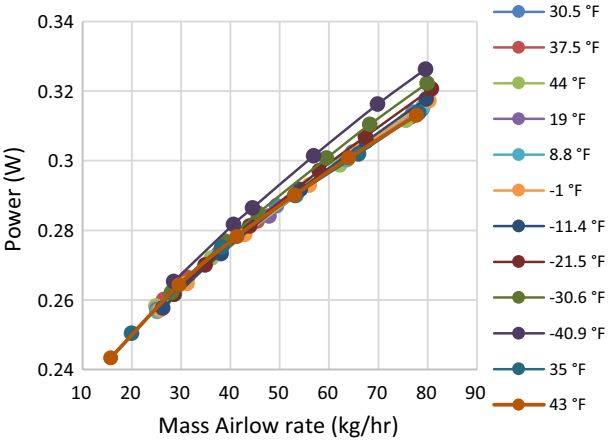

Fig. 8 Measured electrical power versus mass flow rate for ambient temperatures of −40 to 46 °F

Fig. 9 Correlation of the coefficient a(T) and gas temperature for Φ_{hot}

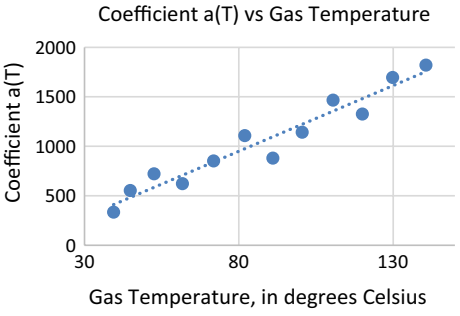

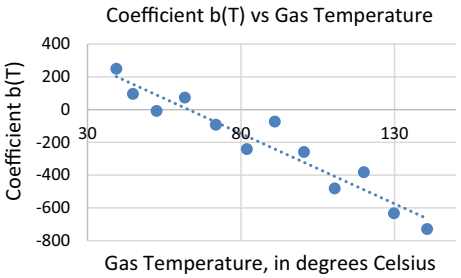

Fig. 10 Correlation of the coefficient b(T) and gas temperature for Φ_{hot}

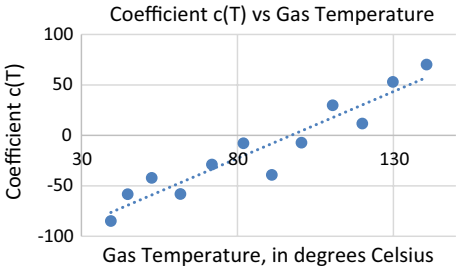

Fig. 11 Correlation of the coefficient c(T) and gas temperature for Φ_{hot}

Table 1 Relationship between the gas temperature and coefficients for Φ_{hot}

T_{gas}, in °F	a(T)	b(T)	c(T)
39.4	334.5427273	249.5007	− 84.8092
44.8	553.2724679	96.17916	− 58.2349
52.5	721.9266025	− 7.86236	− 42.0692
61.7	622.333432	73.51705	− 58.0449
71.8	851.9982062	− 92.281	− 28.8463
81.9	1107.907707	− 240.801	− 7.77311
91	880.4544575	− 73.05	− 39.1156
100.5	1142.1441	− 258.481	− 7.18526
110.5	1466.461002	− 480.942	29.88137
120	1325.964273	− 382.003	11.77329
129.8	1695.664306	− 632.746	53.0458
140.6	1820.311426	− 728.904	70.21021

$$\Phi_{hot} = \left(23.888 \cdot T_A + 313.11\right) \cdot P_e^2 + \left(-15.423 \cdot T_A + 265.12\right) \cdot P_e + \left(2.3809 \cdot T_A - 86.237\right) \tag{21}$$

and

$$\Phi_{cold} = \left(26.932 \cdot T_A + 3244.8\right) \cdot P_e^2 + \left(-12.230 \cdot T_A - 906.87\right) \cdot P_e + \left(1.3672 \cdot T_A + 43.371\right) \tag{22}$$

Table 2 Summary of the Sensor Performance Properties

Thermistor/temperature range	Response time (s)	Maximum full scale error (%)	Range (kg/h)	Resolution (kg/h)
Cold thermistor (−40 to 46 °F)	20	4	[15, 90]	0.42
Hot thermistor (47–140 °F)	16	5.5	[15, 80]	0.2

where $\boldsymbol{\Phi}_{cold}$ and $\boldsymbol{\Phi}_{hot}$ represent the flow rates for ambient temperature from −40 to 46 °F and 46 to 140 °F respectively. Figures 9, 10, and 11 illustrate the relationship between the coefficients and gas temperatures of 46–140 °F for the corresponding data in Table 1. This data was extracted from the expressions of the temperature curves in Fig. 7. Although it is not shown, the same methods were applied to determine the coefficients of $\boldsymbol{\Phi}_{cold}$.

5 Performance Characteristics

The characteristics of the sensor are briefly described in this section. The summary of the performance characteristics is found in Table 2.

5.1 Temperature Range

The MAF sensor was verified for operation in the temperature range between −40 and 140 °F. Two negative temperature coefficient (NTC) thermistors with different resistance properties were utilized as the heated thermistors to extend the operating range of the sensor. To ensure that only one sensor is active at any time, a hysteresis condition was programmed in software to determine which thermistor was activated.

The heated thermistor which operated between 46 and 140 °F had a $B_{25/85}$ parameter of 3600 K within 1%, a dissipation factor 3.5 mW/K, and a resistance at 25 °C of 2.2 kΩ within 5%. The heated thermistor which operated between −40 and 46 °F had a $B_{25/85}$ parameter of 3545 K within 3%, a dissipation factor 2.0 mW/K, and a resistance at 25 °C of 220 Ω within 5%.

These parameters were chosen such that throughout the respective temperature range, the voltage applied to heated thermistors would not saturate at the supply voltage level. Thus, for similar $B_{25/85}$ parameter and dissipation factors the thermistor operating at the higher temperature range had a higher resistance at 25 °C. The $B_{25/85}$ parameter was chosen such that the range of the voltage applied to the heated thermistors was maximized, thus improving the sensitivity and accuracy of the sensor.

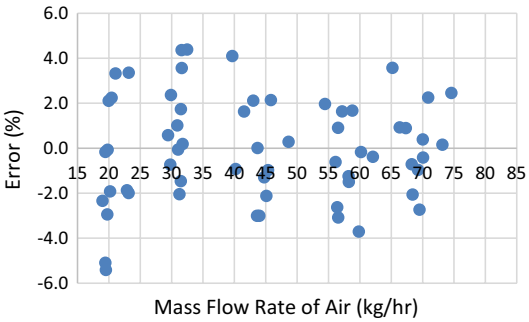

Fig. 12 Error versus mass flow rate for ambient temperatures of 46–140 °F

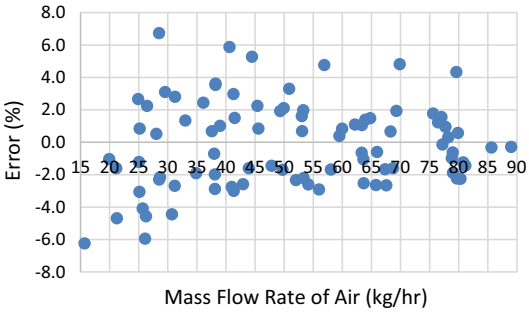

Fig. 13 Error versus mass flow rate for ambient temperatures of − 40 to 46 °F

5.2 Mass Air flow Range

The sensor output has been verified for a range of mass air flow between 15 and 90 kg/h for ambient temperatures between − 40 and 46 °F, and between 15 and 80 kg/h for ambient temperature in the range of 46–140 °F. The maximum air flow is limited by the heated thermistor inability to receive adequate electrical power to heat the thermistor to the desired temperature at extreme ambient temperatures.

5.3 Power Supply Specifications

The nominal operating input voltage for the unit is 24VAC. The maximum operating current was experimentally determined for different testing conditions, and was found to be 120 mA.

5.4 Response Time

The sensor response was found to dependent on the test conditions (ambient temperature, mass flow rate of air, input change) of the system. Experimental response time data was obtained for different flow rate changes. The response time was calculated on the basis of the time required for the response to reach 10–90% of the overall change in flow rate. The average sensor response time was calculated experimentally for different temperature ranges of operation of the sensor and the worst-case results are tabulated in Table 2.

5.5 Accuracy and Precision

The sensor was tested in different environmental conditions (humidity, air pressure, ambient temperature) for different air flow rates. The maximum full-scale error was calculated, and is tabulated in Table 2. Figure 12 illustrates the sensor accuracy for ambient temperatures between 46 and 140 °F, whereas the sensor accuracy for ambient temperatures between − 40 and 46 °F is depicted in Fig. 13.

5.6 Resolution

The resolution of the sensor was dependent upon the resolutions of current and voltage measurements, which were reliant on the resolution of the microcontroller ADC. Furthermore, the resolution of the sensor was also dependent on the calculations of the closed loop PI controller. It was found that the resolution of the sensor is dependent on the ambient temperature and the nominal flow rate. Maximum resolutions were experimentally obtained, and are tabulated in Table 2.

6 Conclusion

A low-cost mass air flow sensor was developed to effectively measure the mass air flow rate for various applications. The slow response time limits the applications that this sensor can be utilized. However, the maximum full-scale error of 5.5%, a range of up to 80 kg/h, and resolution of better than 0.42 kg/h makes this sensor very desirable for applications in combustion burner systems. The sensor relies on laminar flow of debris-free air with minimal disturbances. Therefore, a sensor housing assembly was designed which successfully conditioned the incoming air. The sensor was proven to work effectively with up to 50% blockages of the surface area in the intake air pipe. To improve the performance of the sensor, heated thermistors with a smaller tolerance could be employed. Additionally, the effectiveness of the flow conditioner could be enhanced to better condition the air at turbulent flows.

References

1. Thermal dispersion mass flow. Magnetrol International Incorporated, Downers Grove, IL, 2012 (pp. 11–31).
2. Brooks, E. F., & Barnicoat, G. D. (1981). Air flow measurement techniques for air fuel ratio control. In *31st IEEE vehicular technology conference, 1981* (Vol. 31, pp. 13–18). IEEE. http://ieeexplore.ieee.org/docume-nt/1622906/.
3. Stephan, C. H., & Zanini, M. (1991). A micromachined, silicon mass-air-flow sensor for automotive applications. In *1991 international conference on solid-state sensors and actuators, 1991. Digest of Technical Papers, TRANSDUCERS '91.* San Francisco, CA, USA (pp. 30–33).
4. Sazhin, O. (2013). Novel mass air flow meter for automobile industry based on thermal flow microsensor. I. Analytical model and microsensor. *Flow Measurement and Instrumentation*, *30*, 60–65. http://www.sciencedirect.com/science/article/pii/S0955598613000125.
5. Sazhin, O. (2013). Novel mass air flow meter for automobile industry based on thermal flow microsensor. II. Flowmeter, testprocedures and results. *Flow Measurement and Instrumentation*, *35*, 48–54. http://www.sciencedirect.com/science/article/pii/S0955598613001362.
6. Conte, G., Cesaretti, M., & Scaradozzi, D. (2006). Combustion control in domestic boilers using an oxygen sensor. In *2006 14th mediterranean conference on control and automation*, Ancona (pp. 1–4). https://doi.org/10.1109/med.2006.328702.
7. Kanth, B. B. V., Pavankumar, G. S., Arunkumar, S., & Venkatesan, M. (2014). Design of motor speed control using LabVIEW for air-flow control in wind tunnels. In *2014 IEEE international conference on computational intelligence and computing research (ICCIC),* Coimbatore (pp. 1–4).
8. Bradshaw, P. (1968). Thermal methods of flow measurement. *Journal of Physics E: Scientific Instruments*, *1*(5), 504. http://iopscience.iop.org/-article/10.1088/00223735/1/5/202/pdf.
9. Sosna, C., Buchner, R., & Lang, W. (2010). A temperature compensation circuit for thermal flow sensors operated in constant-temperature-difference mode. *IEEE Transactions on Instrumentation and Measurement*, *59*(6), 1715–1721. http://ieeexplo-re.ieee.org/document/5443848/.
10. Olin, J. G. (1999). Industrial thermal mass flowmeters—Part 1: Principles of operation. *Measurements & Control*, *1*(193), 83–90. http://www.sierrainstruments.com/pr-news/mnc.pdf.
11. Manshadi, M. D., & Esfeh, M. K. (2012). A new approach about heat transfer of hot-wire anemometer. *Applied Mechanics and Materials*, *232*, 747–751. http://www.sc-ientific.net/AMM.232.747.
12. Olin, J.G. (2008). A standard for users and manufacturers of thermal dispersion mass flow meters. Sierra Instruments Inc., Monterey, CA, 2008 (pp. 1–45).
13. Chavan, A. V., Prawdzik, D., Manlove, G., Long, S., Dubois, P., & Dewes, B. (2003). Non-linear temperature compensation for a micromachined bi-directional thermal flow sensor. In *IEEE the sixteenth annual international conference on micro electro mechanical systems, 2003. MEMS-03 Kyoto* (pp. 510–513).